A criterion for the formation of fibrillar layers in injection molded parts

Roberto Pantani[a], Vito Speranza[a]*, Giuseppe Titomanlio[a]

[a]Department of Industrial Engineering, University of Salerno, via Giovanni Paolo II 132, 84084, Fisciano (SA), Italy.

*Corresponding author:

Department of Industrial Engineering, University of Salerno, via Giovanni Paolo II 132, 84084, Fisciano (SA), Italy.

vsperanza@unisa.it

Abstract

It is quite well known that the morphology of an injection molded part made by a semicrystalline polymer presents several layers. In particular spherulitic structures are found in the core region, a layer characterized by highly oriented fibrillar morphology (the shear layer) usually follows and a skin layer is often observed at the sample surface. The thickness of the fibrillar layer deeply influences the mechanical properties of the part. In this work, a criterion to predict the thickness of the fibrillar layer is proposed and verified. The criterion is essentially based on the amount of viscous work done when the molecular stretch is higher than a critical value: the molecular stretch should be above a critical value while a critical amount of viscous work is accumulated. In order to tune the parameters, and to validate the criterion, a well characterized polypropylene was chosen as test material, and four different injection molding conditions were analyzed. The criterion is verified by comparing some experimental results with the prediction of the UNISA code (an injection molding software developed at the University of Salerno), good comparison between software predictions and experimental data confirms the suitability of the criterion.

1 Introduction

The morphology distribution inside an injection molded semicrystalline part is made by several layers moving from the surface toward the midplane: a skin layer, where due to the high cooling rates, the material is quenched and a poorly structured material is found; a shear layer, where due to the strong flow fields highly oriented fibrillar structures are found; a core layer, where spherulitical structures are found, whose dimensions normally increase on increasing the distance from the surface (Karger-Kocsis *et al.*, 1987; Pantani *et al.*, 2005; Balzano *et al.*, 2008; Steenbakkers *et al.*, 2011; Roozemond *et al.*, 2016)

The dependence of the spherulite dimensions upon the processing conditions and their distribution along the thickness of the molded part made of isotactic polypropylene (iPP) have been the object of a series of studies published by the authors in the recent years (Pantani *et al.*, 2016a; Pantani *et al.*, 2017).

The specific work was often considered as the key parameter for the formation of oriented structures in a polymer subjected to a shear field (Janeschitz-Kriegl *et al.*, 2003, 2005). More recently, an attempt was made to determine the criterion which induces the formation of the fibrillar structures. In particular in a previous work on iPP shear induced fibrillar crystallization, a series of experiments were carried out with an iPP (T30G) by a Linkam Cell (Pantani *et al.*, 2010, 2014) within a narrow temperature range around 140°C. It was verified that the material has a limiting shear rate above or below which the crystallization takes place with fibrillar or spherulitic character, respectively. Furthermore, it was found that the shearing time to reach fibrillar crystallization was a decreasing function of the shear rate and, furthermore, the shear stress and the shearing time were found to combine in such a way to give rise to essentially the same viscous work at the start of the fibrillar crystallization. It was also verified that there is a limiting value of shear rate below which the crystallization is spherulitic, whatever amount of viscous work is spent. Those results were taken as further confirmation of the criterion based on a critical work to achieve fibrillar crystallization, as long as the shear rate is larger than a limiting value (Mykhaylyk *et al.*, 2008, 2010; Vega *et al.*, 2009; Fang *et al.*, 2013; Pantani *et al.*, 2014).

In this work, the model for fibrillar crystallization mentioned above is adopted with the following additional simultaneity criterion: the whole amount of work has to be done while the molecular stretch is above a critical value; furthermore, if the molecular stretch is let to relax below that critical value, all previous work has to be cancelled in the accounting for the critical work.

This criterion is consistent with the results of the experiments reported in (Pantani *et al.*, 2010) since the shearing times to achieve fibrillar crystallization were orders of magnitude longer than the resin relaxation time, which implies that most of the viscous work was actually performed when the steady molecular stretch was already achieved.

The injection molding process seems specifically designed to verify the simultaneity criterion clarified above, since soon after filling the polymer not yet solidified relaxes considerable part of its stretch and after a short (but relevant) time it undergoes further stretching with lower shear rate but under higher viscosity due to the temperature decrease and eventually pressure increase. The identification of the thicknesses and the position, within the molded samples cross sections, of the shear layers is the main objective of this work.

2 Injection molding data and process simulation

In the following, the criterion for fibrillar crystallization as outlined above, with the new *simultaneity* criterion, will be applied to the analysis of viscous work and molecular stretch evolutions of four injection molding tests already reported in the literature (Pantani *et al.*, 2005;

Pantani *et al.*, 2007a) carried out by using an iPP (T30G supplied by Basell). The evolutions will be evaluated by the injection molding process model outlined in (Pantani *et al.*, 2016a). The material was injected into a line gated rectangular cavity of 120mm length, 30mm width and 2 mm thickness. Five piezoelectric transducers were placed in the mold along the flow direction: one in the injection chamber, one just before the gate and three in the cavity (at 15, 60 and 105mm downstream from the gate); in the following, the five positions where pressure acquisitions were taken will be referred to as P0, P1, P2, P3 and P4, respectively. Further details on geometry and adopted experimental procedure are available in (Pantani *et al.*, 2005; Pantani *et al.*, 2007a; Speranza *et al.*, 2011).

Those four tests were selected as reference for the fibrillar morphology criterion because they cover injection molding conditions very different one from the other, as specified in Table 1:

	Standard	Slow	High T	High P
Flow rate [cm^3/s]	15	**5**	15	15
Mold temperature [K]	303	303	**343**	303
Holding pressure [bar]	400	400	400	**700**

Tab. 1. Processing conditions for the tests analyzed in this work. The holding time was kept always larger than gate sealing time

In particular, starting from the standard test, all main processing conditions were changed one by one for the other three tests. The effect of molding conditions on the multilayer morphology of injection molded part is evidenced in Fig. 1, where pictures of the samples taken in crossed polarized light are shown. The pictures refer to slices taken in pos P3 (central in cavity), and report just one half of the sample width, with the sample surface at the top, and the midplane at the bottom of the images. In all cases, the flow is parallel to the plane of the slices. In order to clearly identify the position of the layers, beside each optical micrograph a bar reporting the thickness of the skin layer in black, the shear layer in grey and the spherulitic layer in white is shown. The skin layer is clearly evident in all cases except for the High T condition. It is worth mentioning that, according to a detailed characterization of the samples (Pantani *et al.*, 2005), when present, the skin layer is significantly crystalline with a predominance of alpha phase with few percent of mesomorphic phase. The shear layer appears as the darkest part of the pictures; the core layer, that is formed by spherulitic structures with different dimensions, is instead the lightest one. At the midplane, a darker layer is shown in the optical micrograph of all samples considered in this work. Recently (Pantani *et al.*, 2017) a detailed morphological analysis of this layer revealed the presence of spherulites smaller with respect to the adjacent layers. It is evident that the chosen conditions represent a good testing ground for the simulation, since the effect of relevant processing condition on the relative thickness of all the layers is quite clear.
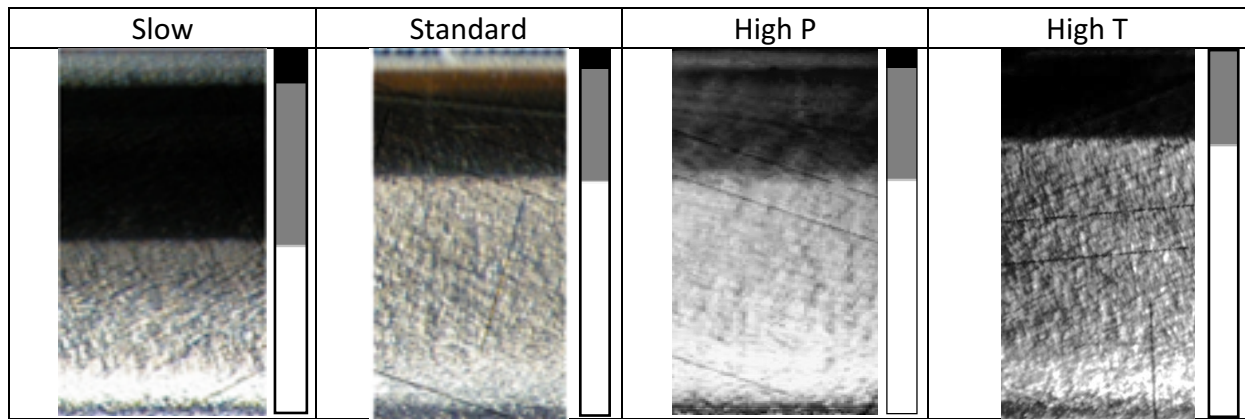
| Slow | Standard | High P | High T |

Fig. 1. Optical images, in cross polarized light, of the half thickness of the sample in position P3 for all the conditions reported in table 1. The sample surface at the top, and the midplane at the bottom of the images. The bar beside each micrograph reports thickness and position of each layer: skin in black, shear in grey and core in white.

The thicknesses of the shear layers and of the skin layer in position P3 of those moldings are reported in Table 2.

	Standard	Slow	High T	High P
Skin layer thickness [µm]	50	80	Not detectable	50
Shear layer thickness [µm]	290	430	250	290

Tab. 2. Thickness of skin and of shear layer for all the conditions considered as measured from optical images reported in fig. 1.

The morphology developed along the sample thickness is due to the balancing between two phenomena: the molecular stretch which takes place mainly during the filling stage and the cooling rate that determines the solidification. Since the structuring is a kinetic process, when the cooling rate through solidification is very high, the material does not have time to achieve a complete structuring. This happens close to the sample surface and determines the skin layer formation. The thickness of the skin layer is expected to decrease as surface cooling rate decreases, as shown in Fig. 1, this happens in the sample sequence conditions Slow, Standard – High P, Hhigh T. The surface cooling rate is expected to be the highest for the slow condition because in that case the convection and viscous generation, being smaller, is less effective to delay the cooling rate through solidification. The sequence of cooling rate among the other conditions is determined by the surface temperature.

3 Injection molding simulation

In the attempt to simulate rheology, crystallinity and molecular stretch evolutions during the injection molding process, all the constitutive equations had to be extrapolated well beyond the experimental ranges, within which each equation had been identified. Details of the constitutive equation adopted (including the values of the constants) are reported in (Pantani *et al.*, 2015a). All the constitutive equations of that iPP resin (T30G) were recently revised (Pantani *et al.*, 2017) on the basis of data published after the publication of the paper which analyzed those injection molding tests for the first time (Pantani *et al.*, 2005; Pantani *et al.*, 2007a).

Numerical simulations of the molding tests were conducted adopting the UNISA code that considers the one–dimension laminar flow of a viscous non–Newtonian fluid in non–isothermal conditions. The wall slip phenomena is not taken into account. The process is considered symmetric with respect to the midplane. In the energy balance, the convective term along the flow direction, the conductive term along the sample thickness, the crystallization latent heat and the viscous generation are considered. A surface heat transfer coefficient is assigned. The geometry is schematized as a series of rectangular or cylindrical elements.

The process is simulated into two stages: filling and packing/cooling. During the filling stage the material is considered incompressible and the flow rate is imposed. The fountain flow is not implemented but the variables at the flow front are averaged on the basis of velocity (i.e. cup-mixing variables are considered at the front). During the packing stage, the material is considered compressible and the flow rate, at each position, is determined by the downstream densification. During the cooling stage the velocity field is annulled and pressure evolution is evaluated on the basis of the PVT behavior of the material accounting of crystallization kinetics.

The effect of flow on crystallization kinetics is accounted through a stretching parameter, as specified elsewhere (Pantani *et al.*, 2017); the equations for the evolution of the stretch parameter are summarized in the section *Definition of the molecular stretch parameter*, reported below. The effects of crystallinity on viscosity and density are taken into account. Consistently, the UNISA code adopts a solidification criterion based on the crystallinity. At last, effect of pressure on viscosity, density and crystallinity are considered. The effect of mold deformation can be accounted for.

The field equations adopted for the numerical simulation are reported in (Titomanlio *et al.*, 1997)(Pantani *et al.*, 2007b) and the capability of the overall model of reproducing main trends of experimental results for both pressure evolutions and of spherulite dimension distribution on the cross section was already verified in a previous paper for the Standard and Slow tests of Table 1 (Pantani *et al.*, 2017). Similar comparison will be considered in this section also for the other two tests.

Afterwards, the thicknesses and the positions of the shear layers, as obtained applying the criterion for the formation of fibrillary morphology (with the *simultaneity* criterion) to the process numerical simulation, will be discussed and compared with the experimental layer thicknesses reported in (Pantani *et al.*, 2005; Pantani *et al.*, 2007a).

Results of the numerical simulation for the tests reported in the previous papers (Pantani *et al.*, 2005; Pantani *et al.*, 2007a) and listed in Table 1 were evaluated with the updated rheology dependencies upon crystallization and with crystallization kinetics including Flow Induced Crystallization (FIC) effects as reported in (Pantani *et al.*, 2015b; Pantani *et al.*, 2016b). Also the effect of mold deformation was accounted for in the simulation, as reported in (Pantani *et al.*, 2007b).

As mentioned above, a comparison between numerical simulation code and experimental results for the pressure evolutions of the Standard and Slow tests was already performed in a previous paper and it was found very good. The comparison for pressure evolutions in the five positions specified above for all the four tests listed in Table 1 is shown in figs. 2a-2d. The comparison indicates that, apart from some discrepancies, which can be surely considered as minor, for the aims of the present work, the simulation well describes the pressure evolutions in all the four molding tests considered.
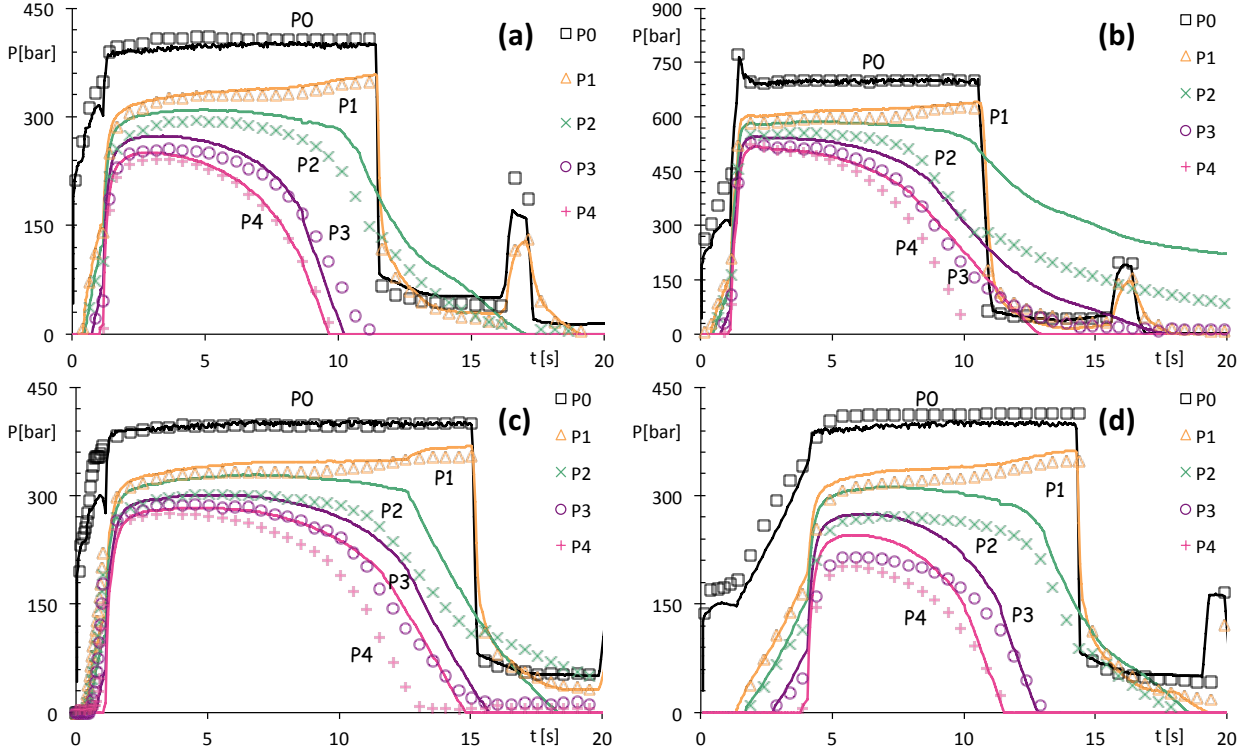
Fig. 2. Comparison of pressure evolutions, acquired in the five positions along the flow path during the process (symbols), with the predicted ones (lines) for all the four conditions reported in table 1. In particular, comparison in (a) is for the "Standard", in (b) is for the "High P", in (c) is for "High T" and in (d) is for "Slow".

3.1 Definition of the molecular stretch parameter

The evolution of molecular stretch was analyzed through the evolution of the molecular conformation tensor $\underline{\underline{A}}$ (Pantani *et al.*, 2012) defined as

$$\underline{\underline{A}} = 3\ \frac{(\langle \underline{RR} \rangle - \langle \underline{RR} \rangle_0)}{\langle R_0^2 \rangle} \tag{1}$$

where $\overline{R}$ is the end-to-end vector of a molecular sub chain, $\langle \overline{R}\,\overline{R} \rangle$ is the second order conformation tensor, $\langle \overline{R}\,\overline{R} \rangle_0$ is the value of the second order conformation tensor under quiescent conditions, when the end-to-end distance of the molecular chain is $\langle R_0^2 \rangle = tr\,\langle \overline{R}\,\overline{R} \rangle_0$. The evolution of the conformation tensor was described by a Maxwell-type equation with a single dominant relaxation time:

$$\frac{D}{Dt}\,\underline{\underline{A}} - \left(\underline{\nabla}\,\underline{v}\right)^T \times \underline{\underline{A}} - \underline{\underline{A}} \times \left(\underline{\nabla}\,\underline{v}\right) = -\frac{1}{\lambda}\,\underline{\underline{A}} + \left(\underline{\nabla}\,\underline{v}\right)^T + \left(\underline{\nabla}\,\underline{v}\right) \tag{2}$$

The dominant relaxation time, λ, decreases when the intensity of the flow field increases according to a Cross-WLF type equation

$$\lambda(T, P, \chi, \Delta) = \frac{\lambda_0 \cdot \alpha(T, P, \chi)}{1 + (a\Delta)^b} \tag{3}$$

where λₒ and Δ are the rest relaxation time and the difference between the two main eigenvalues of the tensor $\underline{\underline{A}}$. A shift factor, α, due to temperature, pressure and crystallinity, χ, is also considered; it is expressed by the modified WLF relationship:

$$\alpha(T,P,\chi) = 10^{\frac{-c_1(T-T_0-C_3P)}{C_2+T-T_0}} \cdot \delta(\chi) \tag{4}$$

where, according to (Pantani *et al.*, 2015a), for the material considered in this work the factor δ is

$$\delta(\chi) = e^{h\chi^2} \tag{5}$$

The values of the material parameters of eq. 3 ÷ 5 were identified in (Pantani *et al.*, 2012; Pantani *et al.*, 2015a) and are reported in Table 3.

Parameter	Value	Parameter	Value
λ_0 [s]	14	C_2 [K]	301.4
T_0 [K]	503.	C_3 [K/bar]	0.18
C_1 [−]	2.5	h [−]	180
a [−]	3.8	b [−]	2.2

Tab. 3. Material parameters adopted in equations 3 ÷ 5 that describe the dependence of relaxation time upon temperature, pressure, crystallinity and molecular stretch.

In this work, the difference, Δ, between the two main eigenvalues of $\underset{\sim}{A}$ is taken as an appropriate measure of the molecular stretch.

Under simple shear the parameter Δ is:

$$\Delta = \sqrt{A_{11}^2 + 4A_{12}^2} \tag{6}$$

Where 1 and 2 are the directions of the gradient of velocity and of the flow.

3.2 Final distributions of stretch and work and their evolutions

Numerical calculations for the integral of the viscous work and for the final stretch distributions of the Standard sample both up to the end of the filling steps (lines) and at the end of the injection molding process (symbols) are plotted in fig. 3 versus the distance from the surface.
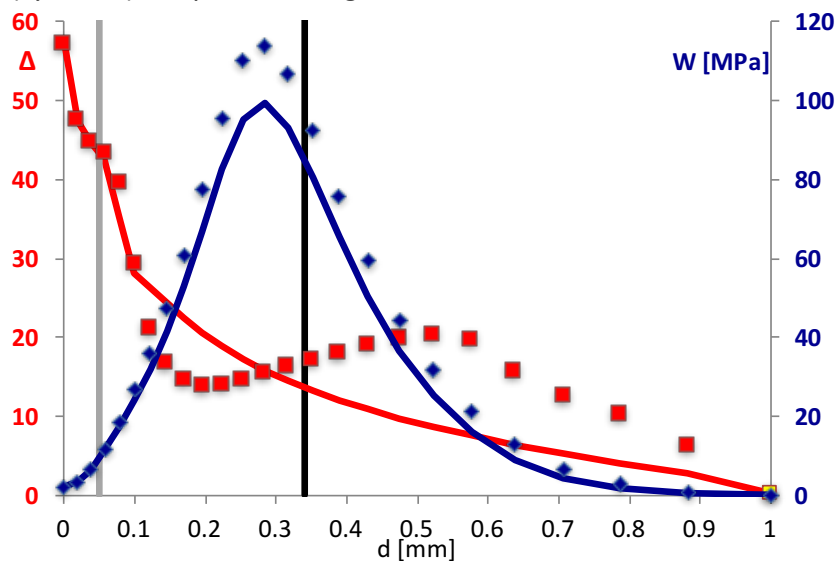

Fig. 3. Integral of the viscous work density (right axis) and molecular stretch parameter Δ (left axis) in position P3, as function of the distance from the surface as calculated for the "Standard" condition. The distribution of both variables at the end of the filling stage (lines) and at the end of the process (symbols) are reported. The thicknesses of the skin and shear layer are indicated as a vertical grey and black line respectively.

The two viscous work curves have regular shapes: the work at surface is very small, it increases toward a maximum (which is at a distance from the surface close to 0.30mm) and then it decreases toward zero, which is reached at the sample mid-plane. The maximum viscous work is between one and two orders of magnitude larger than the value at the surface. The viscous work dissipated up to any instant is the time integral of the viscous work dissipation rate which obviously is positive, thus, due to the packing flow, the viscous work at the end of the process is everywhere (except inside the small layer at the surface, where solidification had taken place during filling) larger than the viscous work at the end of filling. However, because the packing flow is very slow, the difference between the two viscous work curves is quite small except in a narrow zone close to the maxima, although, due to larger pressure and lower temperatures, it takes place under larger viscosity.

The results reported in fig. 3 allow to determine the thickness of the shear layer on the basis of criteria founded on a critical (shear rate) stretch value, Δ_c, and on a critical work value, W_c, as proposed in (Mykhaylyk *et al.*, 2008, 2010): once the critical values of the two parameters are identified, the thickness of the layer is given by all the points presenting both values higher than the chosen thresholds (critical values). This method obviously ignores the *simultaneity* criterion. It can be noticed that, whatever realistic choice would be done for the two critical values, it would not sort a reasonable comparison with the thicknesses and the positions of the shear layers observed in the position P3 of the four injection molding tests, as reported in Tab. 2.

The main objectives of this work is to point out the relevance of the *simultaneity* criterion to the fibrillar crystallization criterion and to compare the experimental and the numerical simulation results for the thicknesses and positions of the fibrillar morphology (shear) layers on the cross sections of the moldings reported in (Pantani *et al.*, 2005; Pantani *et al.*, 2007a).

The criterion that the work performed before the stretch reaches its critical value is not relevant to the purpose of achieving fibrillar crystallization appears physically grounded. In many processing conditions, the polymer melt is oriented first and then has the time to (partially) relax before being oriented again. If the relaxation were complete, it is obvious that the whole previous history does not have any effect of what happens next. This would mean that the time integral of the work alone is not a suitable criterion for describing the phenomenon in complex flow conditions. Considering that, as mentioned above, the criterion without the *simultaneity* criterion is not consistent with the experimental results reported in Table 2, the integral of the viscous work and the final stretch distributions together can be considered a necessary criterion for fibrillar morphology of the polymer, a sufficient criterion needs also the *simultaneity* criterion.

On the other hand in the experiments conducted in (Mykhaylyk *et al.*, 2008, 2010), that consider an isothermal constant rotating parallel-plate flow, under steady shear rate conditions, if transient flow is negligible, the *simultaneity* criterion is automatically assured.

If both the final viscous work integral and the final stretch are above their critical values, the *simultaneity* criterion deny the possibility to have fibrillar morphology if, after the stretch reached its critical value Δ_c, only a quantity of work smaller than the critical one is spent. Similar situations take place very far from the wall, where the stretch undergoes a relevant increase by effect of the packing flow whereas the viscous work, already grown during the filling step, does not undergo enough additional increase after the stretch reached its critical value. With reference to the *Standard* test, considered in Fig 3, the evolutions of the work and of the stretch at the two distances from the surface d=0.12mm and 0.52 mm are very different as far as *simultaneity* although they reach essentially the same value of the final stretch and very similar values of final viscous work. Indeed, the simulation results at 0.12mm from the surface show that the viscous work and the stretch increase simultaneously up to values rather high (those at the end of filling

shown in fig.2), afterwards the stretch undergoes the same relaxation, of about 20% (maintaining a value sufficiently large), and then it undergoes a small stretch recovery to the final value which is reached at about 2 s; at 0.52 mm from the surface most of the viscous work is accumulated during the filling step when the stretch undergoes a moderate increase (because of the high values of the local temperature), vice versa during the packing step there the stretch undergoes a relevant increase and the viscous work increases only marginally, not sufficiently to verify the *simultaneity* criterion if the critical work is larger than about 4MPa .

4 Application of the simultaneity criterion

If the simultaneity criterion is applied, the fibrillar crystalline structures can form when the time integral of the viscous work, calculated when the molecular stretch is constantly larger than Δ_c, reaches a threshold value W_c. If the stretch relaxes below the Δ_c, the work is set to zero again.
The criterion requires thus two critical values (or thresholds): one for the molecular stretch, Δ_c and one for the time integral of the work, W_c.
In fig. 4a – 4d, for the four molding conditions, we report the final distribution along the sample thickness of the work effective, according to the *simultaneity* criterion, calculated for four different choices of the critical stretch: Δ_c=5, 7.5, 8.5 and 10, respectively. The experimentally evaluated thicknesses of the shear layers for each condition are also reported as vertical lines.
It can be noticed that, in the range of the chosen values, the effects of Δ_c can be found only far from the skin. This happens because the molecular stretch at the wall is always very high, and thus all the work done on the melt is useful for the time integral. Closer to the midplane, the molecular stretch is low, and thus a different choice of Δ_c can substantially affect the time integral of the work.
Fig. 4 can be adopted to identify suitable values for Δ_c and W_c. Whatever the value of Δ_c is, the value of W_c should be low, in order to keep the thickness of the skin layer (namely the layer close to the surface in which no fibrillar structures are detected) low. However, if W_c is low, and Δ_c is also low, the predicted thickness of the shear layer would be excessively high for all conditions.
In order to consider both experimental features, it was found that a combination of a Δ_c of about 7 and a W_c of about 10 MPa would provide a good estimation of the layers
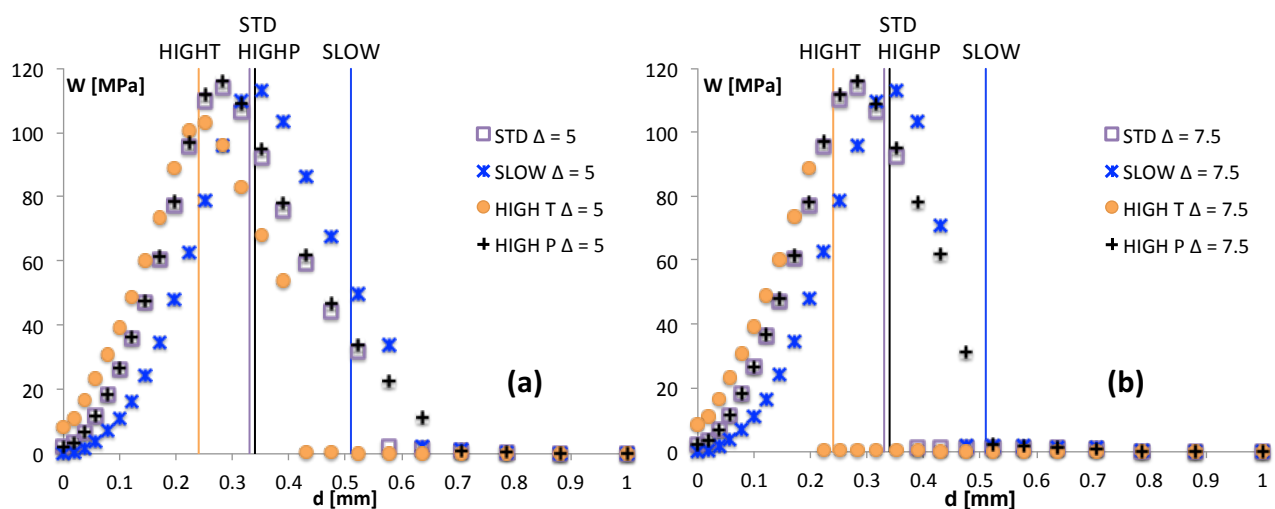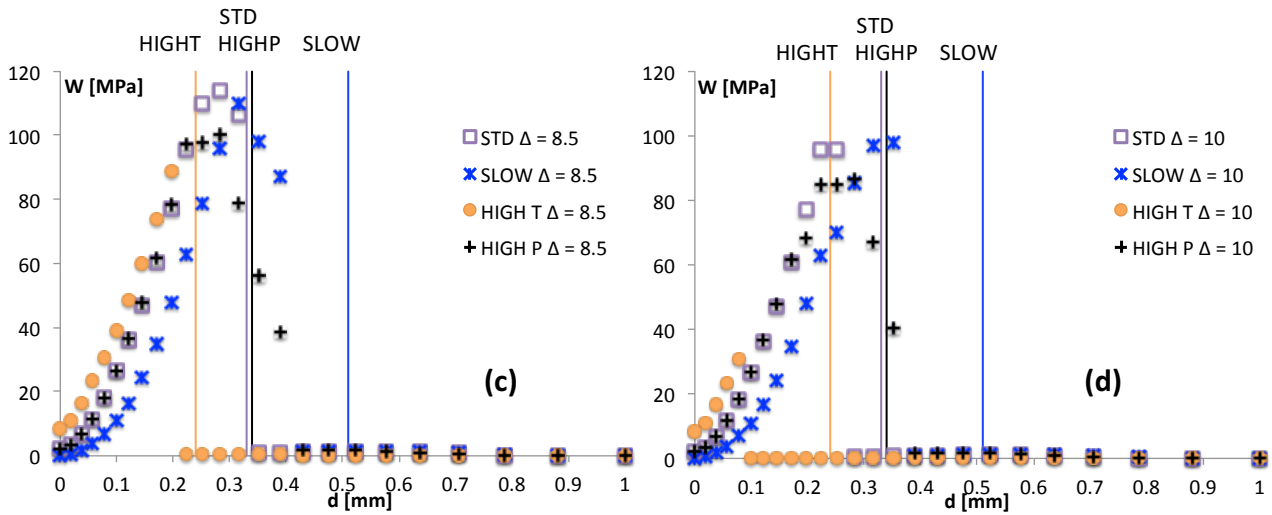
Fig. 4. Final distribution along the sample thickness of the work calculated adopting the simultaneity criterion for different choices of the critical stretch Δ$_c$: in particular Δ$_c$=5 (a), Δ$_c$=7.5 (b), Δ$_c$=8.5 (c) and Δ$_c$=10 (d). The thicknesses of the shear layers for each condition are also reported as vertical lines.

In fig. 5 we report the results of a simulation conducted by using Δ$_c$ = 7 and W$_c$ = 10 MPa. The images of the samples are reported for a visual comparison of the results. It can be noticed that the thicknesses of the skin and of the shear layers are correctly described for all the samples molded with a pressure of 40MPa (namely the standard, high T and slow conditions). An overestimation of the thickness of the shear layer for the sample molded with a pressure of 70MPa (High P) is found. The reasons of this discrepancy can be found in the effect of pressure on viscosity (and on relaxation time) which obviously becomes extremely significant when the pressure levels increase. A deeper analysis of the pressure profiles predicted for this condition (fig. 2b) reveal that the simulated packing phase is longer than what shown by the experiments. This is surely an additional cause of a thicker shear layer for this case.
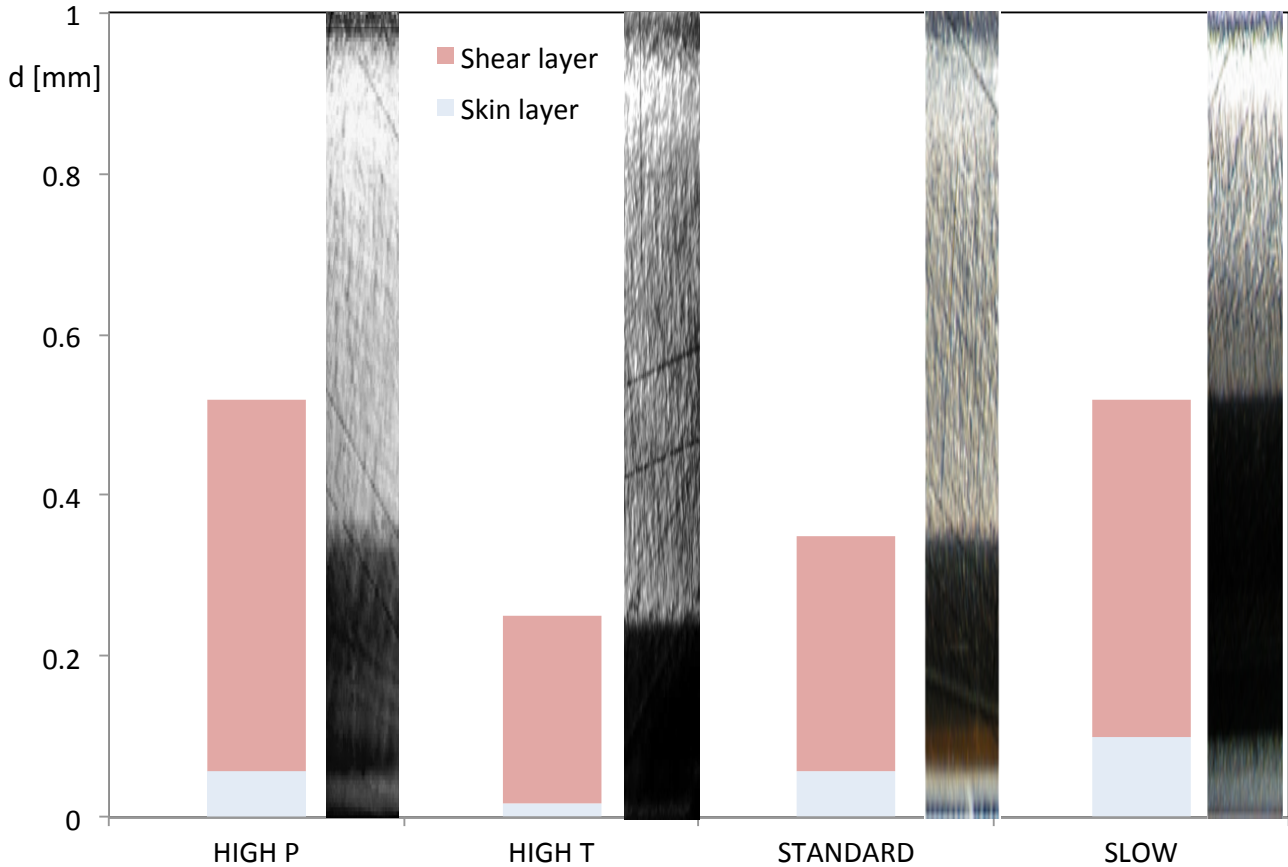
Fig. 5. Comparison between experiments and the results of a simulation conducted by using Δ_c = 7 and Wc = 10 MPa.

5 Conclusions

In this work, a novel criterion is adopted to simulate the occurrence of oriented, fibrillar morphology crystals in semicrystalline polymers. The criterion is based on critical values of the viscous work and of molecular stretch provided the simultaneity of the two occurrences is satisfied: the critical viscous work W_c should be accumulated while the critical molecular stretch $Δ_c$ is already reached.

The criterion is applied to identify the thickness and the position within the cross section of injection molded samples of the fibrillary layer. Four samples obtained with different molding conditions of a well characterized polypropylene have been considered.

In order to predict the shear layer thickness, the injection molding tests were simulated by a software developed at the University of Salerno which is able to considering all the modelling and constitutive aspects needed to describe the phenomena involved: the molecular stretch and the crystallinity evolution, and the mutual effects between crystallinity and flow-fields.

On analyzing the results of the evolution of molecular stretch and viscous work, it was clearly shown that none of the two variable is able alone to describe the thickness of the shear layer. The simultaneity criterion is instead suitable, if appropriate values of $Δ_c$ and W_c are selected. In particular, for the adopted material, by choosing $Δ_c$ = 7 and W_c=10 MPa a satisfactory description of both the skin and the shear layer thickness for all the conditions in which the holding pressure is 40MPa was reached. It is expected that a different material could require different values for $Δ_c$ and W_c.

On comparing the results of the simulation with the experimental data, some discrepancy in the thickness of the shear layer was found for the sample molded with a higher holding pressure (70MPa). In this case, the shear layer was predicted to be larger than the real one. Rather than to

an incorrect criterion for the occurrence of oriented crystals, the discrepancy was ascribed to a non-perfect description of the effect of pressure on viscosity and in general to the fact that the predicted duration of the packing phase in this condition was overestimated. These are aspects to be improved for the simulation of this specific condition.

References

Balzano, L., Rastogi, S. and Peters, G. W. M. "Flow Induced Crystallization in Isotactic Polypropylene–1,3:2,4-Bis(3,4-dimethylbenzylidene)sorbitol Blends: Implications on Morphology of Shear and Phase Separation", Macromolecules. American Chemical Society, **41**(2), 399–408 (2008), DOI: 10.1021/ma071460g

Fang, H., Zhang, Y., Bai, J. and Wang, Z. "Shear-Induced Nucleation and Morphological Evolution for Bimodal Long Chain Branched Polylactide", Macromolecules. American Chemical Society, **46**(16), 6555–6565 (2013), DOI: 10.1021/ma4012126

Janeschitz-Kriegl, H. and Ratajski, E. "Kinetics of polymer crystallization under processing conditions: transformation of dormant nuclei by the action of flow", Polymer, **46**(11), 3856–3870 (2005), DOI: 10.1016/j.polymer.2005.02.096

Janeschitz-Kriegl, H., Ratajski, E. and Stadlbauer, M. "Flow as an effective promotor of nucleation in polymer melts: a quantitative evaluation", Rheologica Acta. Springer-Verlag, **42**(4), 355–364 (2003), DOI: 10.1007/s00397-002-0247-x

Karger-Kocsis, J. and Csikai, I. "Skin-Core morphology and failure of injection-molded specimens of impact-modified polypropylene blends", Polymer Engineering and Science. Society of Plastics Engineers, **27**(4), 241–253 (1987), DOI: 10.1002/pen.760270403

Mykhaylyk, O. O., Chambon, P., Graham, R. S., Fairclough, J. P. A., Olmsted, P. D. and Ryan, A. J. "The Specific Work of Flow as a Criterion for Orientation in Polymer Crystallization", Macromolecules. American Chemical Society, **41**(6), 1901–1904 (2008), DOI: 10.1021/ma702603v

Mykhaylyk, O. O., Chambon, P., Impradice, C., Fairclough, J. P. A., Terrill, N. J. and Ryan, A. J. "Control of Structural Morphology in Shear-Induced Crystallization of Polymers", Macromolecules. American Chemical Society, **43**(5), 2389–2405 (2010), DOI: 10.1021/ma902495z

Pantani, R., Coccorullo, I., Speranza, V. and Titomanlio, G. "Modeling of morphology evolution in the injection molding process of thermoplastic polymers", Progress in Polymer Science, **30**(12), 1185–1222 (2005), DOI: 10.1016/j.progpolymsci.2005.09.001

Pantani, R., Coccorullo, I., Speranza, V. and Titomanlio, G. "Morphology evolution during injection molding: Effect of packing pressure", Polymer, **48**(9), 2778–2790 (2007a), DOI: 10.1016/j.polymer.2007.03.007

Pantani, R., Speranza, V. and Titomanlio, G. "Relevance of Mold-Induced Thermal Boundary Conditions and Cavity Deformation in the Simulation of Injection Molding", Polym Eng Sci, **41**(17), 2022–2035 (2007b)

Pantani, R., Coccorullo, I., Volpe, V. and Titomanlio, G. "Shear-Induced Nucleation and Growth in Isotactic Polypropylene", Macromolecules, **43**, 9030–9038 (2010), DOI: 10.1021/ma101775h

Pantani, R., Speranza, V. and Titomanlio, G. "Orientation distribution in injection molding: A further step toward more accurate simulations", Rheologica Acta, **51**, 1–10 (2012), DOI: 10.1007/s00397-012-0660-8

Pantani, R., Nappo, V., De Santis, F. and Titomanlio, G. "Fibrillar morphology in shear-induced crystallization of polypropylene", Macromolecular Materials and Engineering, **299**(12), 1465–1473 (2014), DOI: 10.1002/mame.201400131

Pantani, R., Speranza, V. and Titomanlio, G. "Simultaneous morphological and rheological measurements on polypropylene: Effect of crystallinity on viscoelastic parameters", Journal of

Rheology, **59**(2), 377–390 (2015a), DOI: 10.1122/1.4906121

Pantani, R., De Meo, A., Speranza, V. and Titomanlio, G. "Effect of Crystallinity on the Viscosity of an Isotactic Polypropylene", AIP Conference Proceeding. Polymer Processing with Resulting Morphology and Properties, **1695**, 20065-1-6 (2015b), DOI: 10.1063/1.4937343

Pantani, R., Speranza, V. and Titomanlio, G. "Thirty Years of Modeling of Injection Molding. A Brief Review of the Contribution of UNISA Code to the Field", International Polymer Processing, **31**(5), 655–663 (2016a), DOI: 10.3139/217.3249

Pantani, R., Santis, F. De, Speranza, V. and Titomanlio, G. "Analysis of fl ow induced crystallization through molecular stretch", Polymer. Elsevier Ltd, **105**, 187–194 (2016b), DOI: 10.1016/j.polymer.2016.10.026

Pantani, R., Speranza, V. and Titomanlio, G. "Effect of flow-induced crystallization on the distribution of spherulite dimensions along cross section of injection molded parts", European Polymer Journal, **97**, 220–229 (2017), DOI: 10.1016/j.eurpolymj.2017.10.012

Roozemond, P. C., van Drongelen, M. and Peters, G. W. M. "Modeling Flow-Induced Crystallization", in Advances in Polymer Science. Springer, Cham, 243–294 (2016), DOI: 10.1007/12_2016_351

Speranza, V., Vietri, U. and Pantani, R. "Monitoring of injection molding of thermoplastics: Average solidification pressure as a key parameter for quality control", Macromolecular Research, **19**(6), 542–554 (2011), DOI: 10.1007/s13233-011-0610-9

Steenbakkers, R. J. A. and Peters, G. W. M. "A stretch-based model for flow-enhanced nucleation of polymer melts", Journal of Rheology. The Society of Rheology, **55**(2), 401–433 (2011), DOI: 10.1122/1.3545844

Titomanlio, G., Speranza, V. and Brucato, V. "On the simulation of thermoplastic injection moulding process: II Relevance of interaction between flow and crystallization", International Polymer Processing, **12**(1), 45–53 (1997), DOI: 10.3139/217.950055

Vega, J. F., Hristova, D. G. and Peters, G. W. M. "Flow-induced crystallization regimes and rheology of isotactic polypropylene", Journal of Thermal Analysis and Calorimetry. Springer Netherlands, **98**(3), 655–666 (2009), DOI: 10.1007/s10973-009-0516-3

Captions for the Figures

Fig. 1. Optical images, in cross polarized light, of the half thickness of the sample in position P3 for all the conditions reported in table 1. The sample surface at the top, and the midplane at the bottom of the images. The bar beside each micrograph reports thickness and position of each layer: skin in black, shear in grey and core in white.

Fig. 2. Comparison of pressure evolutions, acquired in the five positions along the flow path during the process (symbols), with the predicted ones (lines) for all the four conditions reported in table 1. In particular, comparison in (a) is for the "Standard", in (b) is for the "High P", in (c) is for "High T" and in (d) is for "Slow".

Fig. 3. Integral of the viscous work density (right axis) and molecular stretch parameter Δ (left axis) in position P3, as function of the distance from the surface as calculated for the "Standard" condition. The distribution of both variables at the end of the filling stage (lines)

and at the end of the process (symbols) are reported. The thicknesses of the skin and shear layer are indicated as a vertical grey and black line respectively.

Fig. 4. Final distribution along the sample thickness of the work calculated adopting the simultaneity criterion for different choices of the critical stretch Δ_c: in particular Δ_c=5 (a), Δ_c=7.5 (b), Δ_c=8.5 (c) and Δ_c=10 (d). The thicknesses of the shear layers for each condition are also reported as vertical lines.

Fig. 5. Comparison between experiments and the results of a simulation conducted by using $\Delta_c = 7$ and $W_c = 10$ MPa.
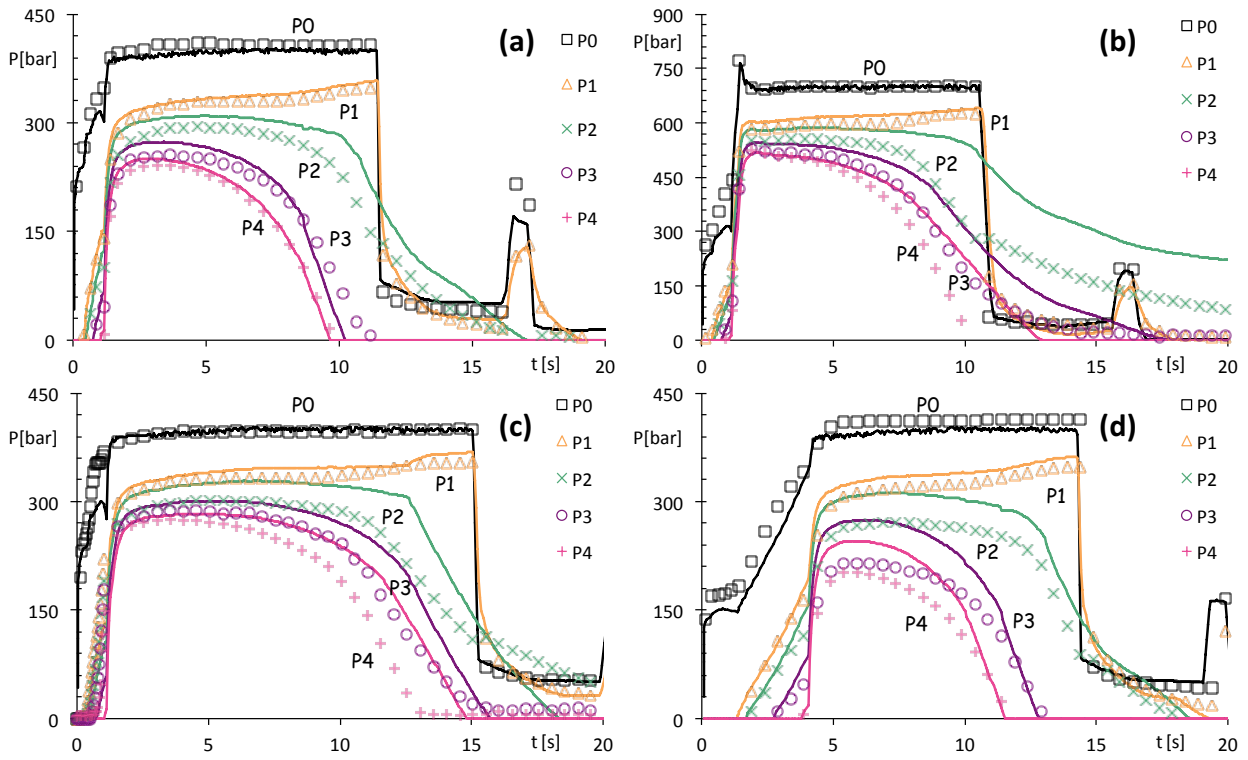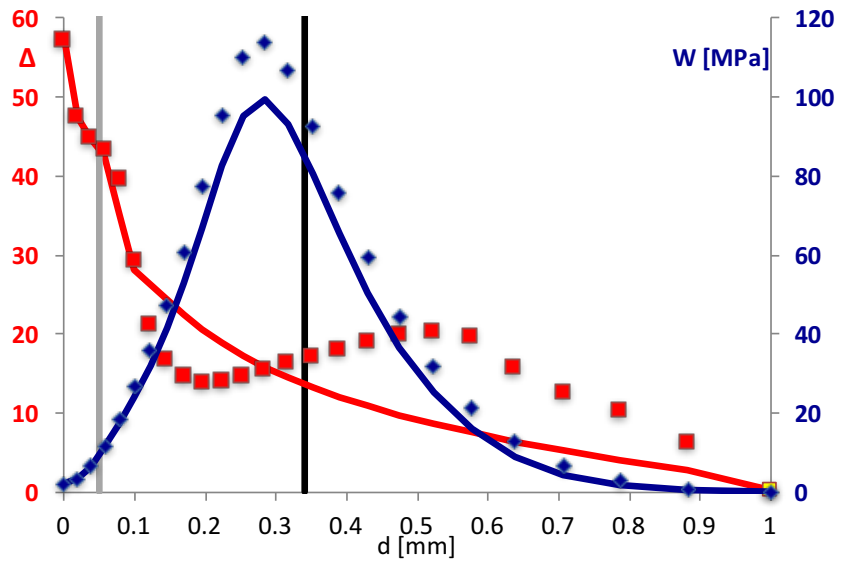
Figures

Slow	Standard	High P	High T

Fig. 1.

Fig. 2.

Fig. 3.

Fig. 4.

Fig. 5.